Magnetotransport properties of the single-crystalline nodal-line semimetal candidates CaTX(T=Ag,Cd;X=As,Ge)

Eve Emmanouilidou, Bing Shen, Xiaoyu Deng, Tay-Rong Chang, Aoshuang Shi, Gabriel Kotliar, Su-Yang Xu, and Ni Ni

Phys. Rev. B **95**, 245113 — Published 14 June 2017

DOI: 10.1103/PhysRevB.95.245113

Magnetotransport properties of the single-crystalline nodal-line semimetal candidates CaTX (T=Ag, Cd; X=As, Ge)

Eve Emmanouilidou,[1,*] Bing Shen,[1,*] Xiaoyu Deng,[2] Tay-Rong Chang,[3] Aoshuang Shi,[1] Gabriel Kotliar,[2] Su-Yang Xu,[4] and Ni Ni[1,†]

[1] *Department of Physics and Astronomy and California NanoSystems Institute, University of California, Los Angeles, CA 90095, USA*
[2] *Department of Physics and Astronomy, Rutgers University, Piscataway, NJ 08854, USA*
[3] *Department of Physics, National Cheng Kung University, Tainan, 701, Taiwan*
[4] *Department of Physics, MIT, Cambridge, MA 02139, USA*

Topological semimetals are characterized by protected crossings between conduction and valence bands. These materials have recently attracted significant interest because of the deep connections to high-energy physics, the novel topological surface states, and the unusual transport phenomena. While Dirac and Weyl semimetals have been extensively studied, the nodal-line semimetal remains largely unexplored due to the lack of an ideal material platform. In this paper, we report the magnetotransport properties of the two nodal-line semimetal candidates CaAgAs and CaCdGe. First, the transport properties of our single crystalline CaAgAs agree with those of CaAgAs polycrystals. They can be explained by the single-band model, consistent with the theoretical proposal that only non-trivial Fermi pockets linked by the topological nodal-line are present at the Fermi level. Second, our CaCdGe sample provides an ideal platform to perform comparative studies because the theoretical calculation shows that it features the same topological nodal line but has a more complicated Fermiology with irrelevant Fermi pockets. As a result, the magnetoresistance of our CaCdGe sample is more than 100 times larger than that of CaAgAs. Through our systematic magnetotransport and first-principles band structure calculations, we show that our CaTX compounds can be used to study, isolate, and control the novel topological nodal-line physics in real materials.

I. INTRODUCTION

Understanding the nontrivial topological properties in electronic band structures has become one of the central themes in condensed matter physics and materials science. Following the discovery of the 2D quantum Hall effect, the quantum spin Hall effect and 3D topological insulators[1–4], interest has recently shifted toward realizing topological physics in gapless systems, i.e., topological semimetals. Topological semimetals are characterized by robust bulk band crossing points and the associated topological boundary states. They can be classified by the dimension of the band crossing in momentum space. Two prominent examples of topological semimetals with 0D band crossing points are the Dirac and Weyl semimetals. Their realizations in Na_3Bi[5,6], Cd_3As_2[7,8], TaAs[9,10] and related materials have attracted enormous interest worldwide.

The other type of topological semimetal is the nodal-line semimetal whose conduction and valence bands cross to form a 1D closed loop in momentum space. The nodal-line semimetal differs from the Weyl semimetal in three aspects : (1) the bulk Fermi surface is 1D in nodal-line and 0D in Dirac/Weyl semimetals ; (2) the density of states near the nodal touchings is proportional to $|E-E_{\mathrm{F}}|^2$ in nodal-line and $|E-E_{\mathrm{F}}|$ in Weyl semimetals ; (3) on the surface, the nodal-lines are "stitched" together by a "drumhead" surface state, while Weyl nodes are connected by Fermi arc surface states. These unique properties of nodal-line semimetals make new physics accessible. For example, the weak dispersion of the drumhead surface states leads to a large density of states near the Fermi level. Therefore, possible interaction-induced instabilities on the surface of nodal-line semimetals have been widely discussed in theory[11–13].

Despite intense theoretical interest[14–21], there haven't been many experimental studies on nodal-line semimetals. A major reason is the lack of ideal nodal-line semimetal materials, where only the nodal lines are present at the Fermi level with minimal irrelevant Fermi pockets. Such a "hydrogen atom" nodal-line semimetal is crucial for isolating the spectroscopic and transport signals of the nontrivial nodal lines from those of trivial states. For example, even before the discovery of TaAs, Fe, an elemental ferromagnetic metal, was known to have hundreds of Weyl nodes in its band structure[22] . However, Fe is not an ideal platform to study Weyl physics because its complicated Fermi surface is dominated by irrelevant (non-Weyl) trivial pockets. In fact, because Weyl nodes are symmetry allowed when time-reversal or inversion symmetry are broken, they are likely to exist in the band structure of most ferromagnetic or non-centrosymmetric compounds. In this sense, the key is to identify a material where the topological band crossings (Dirac nodes, Weyl nodes, or nodal lines) are the dominant features at the Fermi level. Since such a platform is accessible in Dirac and Weyl semimetals (Cd_3As_2, Na_3Bi and TaAs), these topological materials have been studied extensively and novel physics has been discovered. By contrast, in nodal line semimetals, experimental work has been focused on $PbTaSe_2$ and ZrSiX (X=S, Se, Te)[23,24]. However, it is well-understood that both compounds have a quite complex band structure where multiple irrelevant pockets coexist with the nodal lines at the Fermi level.

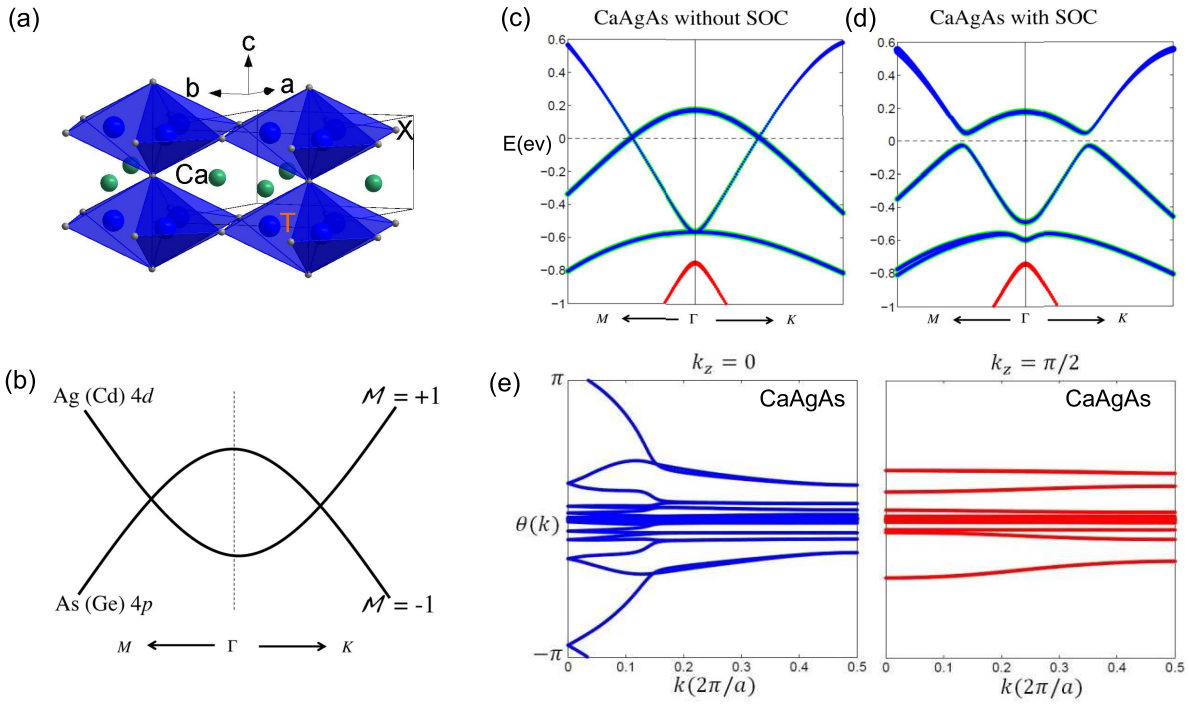

FIG. 1. (a) Crystal structure of CaAgAs and CaCdGe. TX_4 octahedra are shown in blue. Ca atoms are shown in green. (b)-(c): Mirror symmetry protected nodal-lines in CaAgAs and CaCdGe: (b) Schematic of a band structure diagram for the nodal-line feature in CaAgAs and CaCdGe. The conduction and valence bands are made up of the Ag(Cd) 4*d* and As(Ge) 4*p* orbitals respectively. The band crossings near the Γ point are protected because these two bands have opposite mirror eigenvalues. (c,d) First-principles calculated band structures of CaAgAs near the Γ point without SOC (c) and with SOC (e) Wilson loop calculation of the SOC band structure on the $k_z = 0$ and $k_z = \pi/2$ planes.

The noncentrosymmetric CaAgX (X=As, P) compound crystalizing in the P-62m space group[25] was recently proposed to be a "hydrogen atom" nodal-line semimetal where two non-trivial bulk bands touch along a line and no trivial bands exist at the FL[26]. The crystal structure is shown in Fig. 1(a). It consists of a 3D-network of edge and corner sharing $AgAs_4$ tetrahedra. A recent study on polycrystalline CaAgX (X=As, P) revealed that it is a low carrier density metal and that CaAgAs is a more promising candidate than CaAgP for the purpose of studying the nodal lines[27]. Compared to polycrystals, single crystals are superior for transport studies and surface sensitive measurements. Until now however, no studies of single crystalline CaAgAs have been reported. In this paper, we report the magneto-transport properties of CaAgAs and its sister compound CaCdGe. CaCdGe also crystalizes in the P-62m space group[28], featuring the same topological nodal line but with a much more complicated Fermiology, providing an ideal platform to perform comparative studies. We show that such a comparative study sheds light on a novel transport phenomenon prominently observed in many topological semimetals, the giant magnetoresistance.

II. EXPERIMENTAL METHODS

CaAgAs crystals were grown with AgAs flux while CaCdGe crystals were grown using Cd flux. Ca granules and AgAs powder were mixed at a molar ratio of Ca:AgAs=1:4; Ca, Ge and Cd granules were mixed at a ratio of Ca:Ge:Cd=1:1:47. The materials were loaded into alumina crucibles and then sealed inside quartz tubes under 1/3 ATM of Ar. For CaAgAs, the ampoule was heated to 1100°C, kept at that temperature for 3 hours, and cooled to 750°C at a rate of 3°C/hour. For CaCdGe, the ampoule was heated to 800°C or 1000°C for 3 hours and cooled to 400°C at a rate of 3°C/hour. For CaCdGe, to compensate for the vaporized Cd in the growths which went up to 1000°C, 25% extra Cd was added. These growths yielded much larger single crystals while the growths going up to 800°C yielded smaller needle-like single crystals with higher residual resistivity ratio (RRR). In both cases, the single crystals were separated from the flux by centrifuging.

X-ray diffraction measurements were performed using a PANalytical Empyrean (Cu Kα radiation) diffractometer. Magnetotransport measurements were performed using a Quantum Design Physical Property Measurement System (QD PPMS Dynacool). The excitation current I was set to 1-2 mA and along the c axis, and magnetic

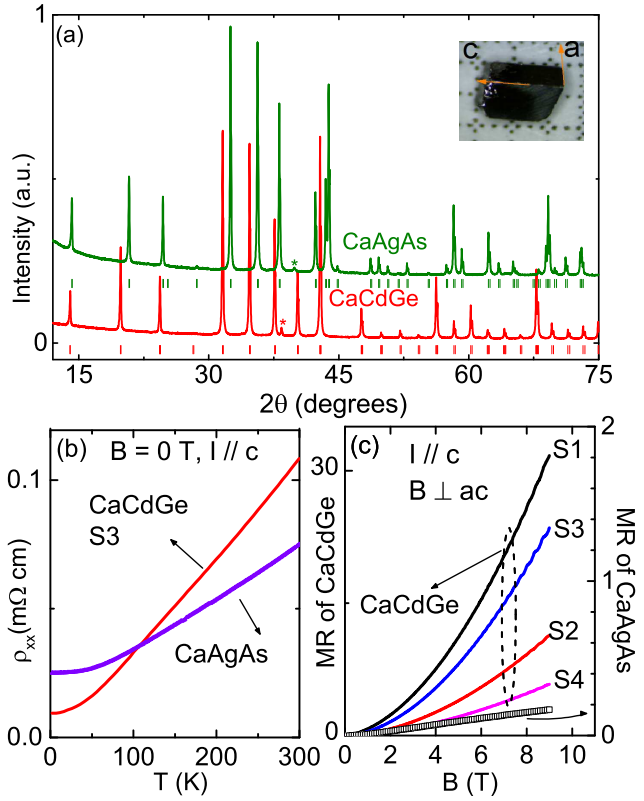

FIG. 2. (a) The powder x-ray diffraction patterns of CaCdGe and CaAgAs. The ticks below each pattern indicate the Bragg peak positions determined by the respective crystal structure. The impurity peak marked with an asterisk in the CaCdGe pattern is from Cd while the one in CaAgAs is from CaAs. Inset: CaCdGe single crystal on a mm scale. The crystalline directions are shown. (b) Temperature dependence of the electrical resistivity ρ_{xx} for CaCdGe and CaAgAs at $B = 0$ T with $I//c$. (c) MR of CaCdGe and CaAgAs single crystals at T= 2 K with $I//c$ and $B \perp ac$.

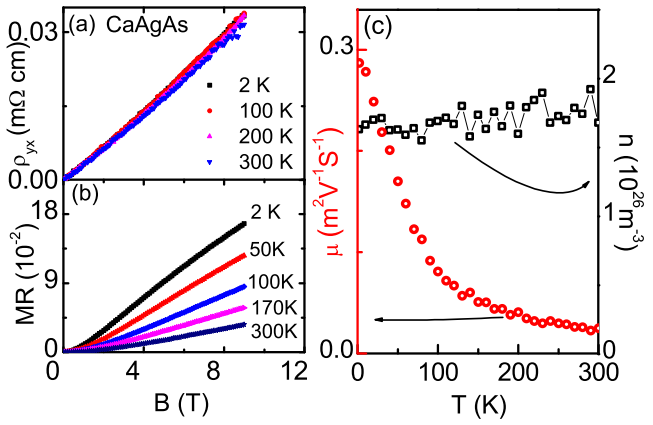

FIG. 3. CaAgAs single crystal with $I//c$ and B $\perp$ ac: (a) Hall resistivity ρ_{yx}. (b) Field dependent transverse MR. (c) Temperature dependent carrier density and mobility.

fields up to 9 T were applied. We used the standard four- and six- probe techniques to measure the electrical resistivity ρ_{xx} and Hall resistivity ρ_{yx} with $\rho_{xx}(B) = \frac{\rho_{xx}(B)+\rho_{xx}(-B)}{2}$ and $\rho_{yx} = \frac{\rho_{yx}(B)-\rho_{yx}(-B)}{2}$ respectively. The electronic structure of CaCdGe was studied using first principles calculations based on density functional theory and the full-potential linear augmented plane wave method as implemented in the Wien2k package[29,30]. Spin orbit coupling (SOC) was taken into account in the calculation. The local density approximation (LDA) and the Tran-Blaha modified Becke-Johnson (MBJ)[31] exchange potential were used in our calculations.

III. EXPERIMENTAL RESULTS AND DISCUSSION

The valence analysis (Ca^{2+}, Ag^{1+}, As^{3-} for CaAgAs and Ca^{2+}, Cd^{2+}, Ge^{4-} for CaCdGe) suggests a semimetal/semiconductor ground state for both compounds, which is confirmed by our band structure calculations. As shown in Fig. 1(c), the conduction and valence bands cross in the absence of SOC. The energy dispersion around E_F is nearly linear. The band crossing forms a 1D loop (a nodal-line) that encloses the Γ point.

We now move on to explain the existence of the nodal line near the Fermi level (Fig. 1(b)). Our calculation shows that near the Γ point, the lowest conduction and valence bands are made up of the Ag(Cd) 4d and As(Ge) 4p orbitals, respectively. At the Γ point, a band inversion takes place as the top of the valence (As 4p) band moves above the bottom of the conduction (Ag 4d) band. Furthermore, because the $z = 0$ plane of the crystal is a mirror plane, the electron states on the $k_z = 0$ plane must be eigenstates of the mirror operation $\mathcal{M}_z$, which takes z to $-z$. Interestingly, the Ag 4d conduction band and the As 4p valence band have opposite mirror eigenvalues. This fact prevents them from hybridizing, leading to a nodal-line on the $k_z = 0$ plane enclosing the Γ point. Upon the inclusion of SOC, a gap of less than 20 meV opens (Fig. 1(d)), which is much smaller than the band width (1 eV). This gap is topologically nontrivial. This can be clearly seen in the Wilson loop calculation of the SOC band structure on the $K_z = 0$ and $K_z = \Pi/2$ planes shown in Fig. 1(e). Therefore, both CaAgAs and CaCdGe compounds can be regarded as nodal-line semimetals if the Fermi level is located away from the gap. We noticed that the same issue (SOC opening a gap) applies to almost all other "Dirac" line-node semimetals including graphene networks, Ca_3P_2, LaN, Cu_3(Pd,Zn)N, and ZrSiX.

Figure 2(a) shows the powder x-ray diffraction patterns of CaCdGe and CaAgAs. The impurity peak marked with $*$ in the CaCdGe pattern is from Cd while the one in CaAgAs is from CaAs. Based on the Rietveld refinement of the powder x-ray diffraction data, the lattice parameters are $a = b = 7.3056(1)$Å, $c = 4.4785(1)$Å

for CaCdGe, and $a = b = 7.2041(1)$Å, $c = 4.2699(1)$Å for CaAgAs. As a representative, the inset of Fig. 2(a) shows the sample orientation of a CaCdGe single crystal with the as-grown rectangular surface as the *ac* plane and the hexagonal as-grown cross section as the *ab* plane. CaCdGe and CaAgAs both demonstrate metallic behavior, as can be seen in Fig. 2(b). The RRR is 3 with a residual resistivity ρ_0 of 25 $\mu\Omega$ cm for CaAgAs and 12 with a ρ_0 of 9 $\mu\Omega$ cm for CaCdGe. Figure 2(c) shows the transverse magnetoresistance (MR) of four CaCdGe samples, and one representative CaAgAs sample. CaCdGe exhibits large, quadratic-like MR without a sign of saturation up to 9 T. S1 in particular, has an MR around 3200% at 2 K under 9 T. This behavior is reminiscent of the extremely large MR recently observed in materials such as the Weyl semimetals TaAs and NbP, the type II-Weyl semimetal WTe_2, the Dirac semimetal Cd_3As_2 and the weak topological insulator $NbAs_2$[32–39]. In sharp contrast to the giant quadratic MR of CaCdGe, the MR of CaAgAs only goes up to about 18% and most notably has a non-quadratic character, which agrees with the recent work on polycrystalline CaAgAs[27].

Figure 3(a) shows the Hall resistivity ρ_{yx} for CaAgAs, which appears to be positive. It is linear with applied field up to 9 T and shows almost no temperature dependence, indicating that hole carriers overwhelmingly dominate the electrical transport. This is indeed consistent with the theoretical prediction that only one Fermi pocket exists at the FL[26]. Figure 3(b) shows the MR of CaAgAs for some representative temperatures. While quadratic at small magnetic fields, it develops a linear behavior at high fields. Linear MR has also been observed in the topological semimetals Na_3Bi[40], WTe_2[39] and Cd_3As_2[34,38,41] that have linear energy-momentum dispersions, as well as materials with parabolic dispersions such as $Ag_{2-\delta}Se$[43] or the GaAs quantum well[44], and recently in the candidate topological superconductor Au_2Pb[42] . Despite being a subject of study for decades, its origin is still under debate[44,45]. Using $n = B/e\rho_{yx}$ and $\mu = R_H\sigma_{xx}$, the temperature dependent carrier density n and mobility μ were estimated and are shown in Fig. 3(c). n is temperature independent and is of the order of 1.7×10^{26} m^{-3} while μ shows a strong temperature dependence ranging from 0.3 m^{2}V^{-1}s^{-1} at 2 K, to 0.025 m^{2}V^{-1}s^{-1} at 300 K.

As presented in Fig. 2(c), CaAgAs and CaCdGe show quite different behavior under magnetic field. In order to understand the origin of the large non-saturating MR observed in CaCdGe, we performed temperature dependent magnetotransport measurements. As a representative, the data measured on S3 with I // c and B $\perp$ *ac* are shown in Fig. 4. The transverse magnetoresistivity has a quadratic dependence on magnetic field (Fig. 4(a)). The pattern of the Hall resistivity ρ_{yx} evolves with temperature and deviates from linear behavior at temperatures below 100 K (Fig. 4(b)). This suggests that transport in this compound is governed by both electron and hole carriers. To get a quantitative estimation of the carrier

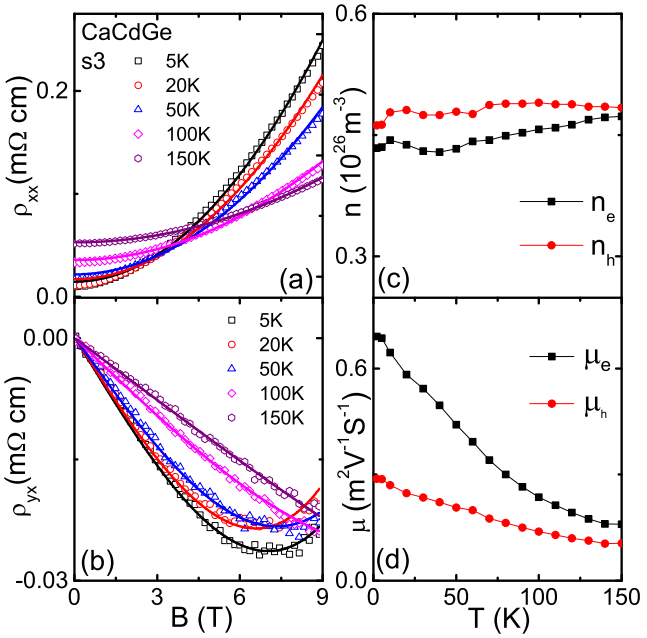

FIG. 4. CaCdGe single crystal s3 with $I//c$ and B $\perp$ *ac*: (a) Transverse magneto-resistivity ρ_{xx}. (b) Hall resistivity ρ_{yx}. The symbols correspond to experimental data, while the lines are the curves obtained from the two band model fitting. (c) Temperature dependent carrier densities. (d) Temperature dependent mobilities.

densities and mobilities in CaCdGe, we used the semi-classical two band model to analyze the data[36,46]. The field dependencies of ρ_{xx} and ρ_{yx} are given by

$$\rho_{xx} = E_x/J_x = \frac{n_e\mu_e + n_h\mu_h + (n_e\mu_h + n_h\mu_e)\mu_e\mu_h B^2}{e(n_e\mu_e + n_h\mu_h)^2 + e(n_h - n_e)^2\mu_e^2\mu_h^2 B^2} \quad (1)$$

and

$$\rho_{yx} = E_y/J_x = \frac{B(n_h\mu_h^2 - n_e\mu_e^2) + (n_h - n_e)\mu_e^2\mu_h^2 B^3}{e(n_e\mu_e + n_h\mu_h)^2 + e(n_h - n_e)^2\mu_e^2\mu_h^2 B^2} \quad (2)$$

where n_e, n_h, μ_e and μ_h are the fitting parameters, representing the carrier densities and mobilities of electrons and holes respectively. Simultaneously fitting our data with Eq. (1) and (2) allows us to determine the temperature dependencies of n_e, n_h, μ_e and μ_h. The fitting curves are presented as lines in Fig. 4 (a) and (b) and agree well with the experimental data. Figures 4 (c) and (d) show the temperature dependent n_e, n_h, μ_e and μ_h inferred from the fits. Both values of n_e and n_p are very similar to each other, being around $n \sim 5 \times 10^{25}$/m^3 and showing almost no temperature dependence. This suggests that the large non-saturating MR comes from the electron-hole compensation effect. Both μ_e and μ_h (Fig. 4(d)) increase with decreasing temperatures, being consistent with the weaker scattering at lower temperatures. At 2 K, μ_e is 0.7 m^2/V/S while μ_h is 0.3 m^2/V/S.

In CaCdGe, Shubnikov-de Haas (SdH) oscillations were observed above 6 T in ρ_{xx}, as shown in Fig. 2(c).

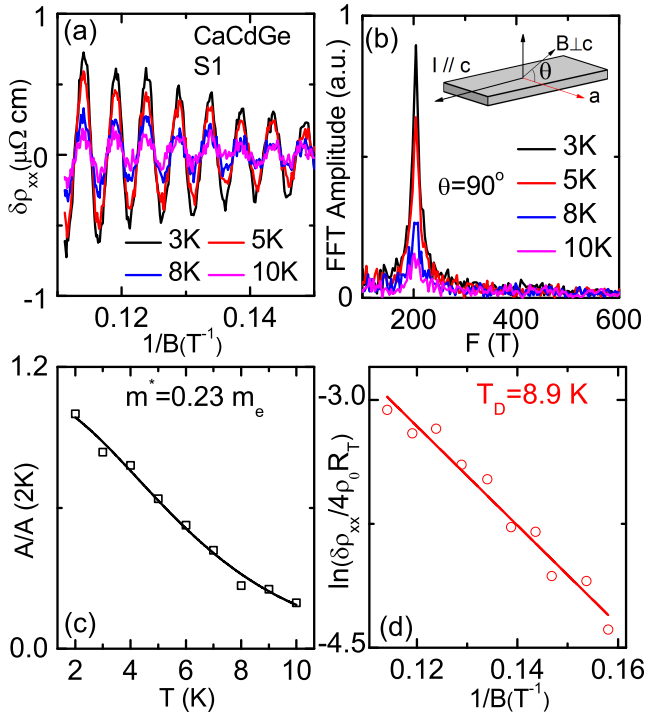

FIG. 5. (a) The oscillating part of ρ_{xx}, $\delta\rho_{xx}$, vs. 1/B. (b) FFT spectrum of $\delta\rho_{xx}$ for a few representative temperatures. Inset : Measurement configuration. The magnetic field was normal to the *ac* plane. (c) Temperature dependence of the normalized amplitude of $\delta\rho_{xx}$ denoted as A/A(2K). (d) 1/B dependence of the quantity $ln(\delta\rho_{xx}/4\rho_0 R_T)$, where $R_T = \frac{\alpha T m^*/B}{sinh(\alpha T m^*/B)}$, used to extract the Dingle temperature.

These oscillations are a result of the singularity in the density of states at the FL that occurs every time a Landau level crosses the FL. We analyzed the SdH data by first subtracting a polynomial background and then plotting $\delta\rho_{xx} = \rho_{xx} - \rho_{bkg}$ as a function of 1/B. Figure 5(a) shows $\delta\rho_{xx}$ for S1 as a function of 1/B at a few representative temperatures with I // c and B⊥ ac. The oscillations are periodic in 1/B. Their frequency F is related to the extremal cross sectional area S of the Fermi surface perpendicular to the magnetic field through the Onsager relation $F = \hbar S/2\pi e$[46]. The Fast Fourier Transform (FFT) spectrum of the oscillations reveals only one frequency around 204 T, which is labelled as F_a^{SdH} and shown in Fig. 5 (b). The amplitude of the oscillations, taking finite temperature and impurity scattering effects into account, is described by the Lifshitz-Kosevich formula

$$\frac{\delta\rho_{xx}}{4\rho_0} = \exp(-\alpha T_D m^*/Bm_e)\frac{\alpha T m^*/Bm_e}{sinh(\alpha T m^*/Bm_e)} \quad (3)$$

where $T_D = \hbar/(2\pi k_B \tau_q)$ is the Dingle temperature, related to the quantum lifetime $\tau_q = \hbar/2\pi k_B T_D$, $\alpha = 2\pi^2 k_B m_e/\hbar = 14.69$ T/K, m^* is the effective mass and m_e the electron mass[46].

Using this formalism, we extracted an effective mass m^* of $0.23m_e$ (Fig. 5(c)). It is worth noting that for CaCdGe at 2 K and 9 T, $\hbar\omega_c = \hbar eB/m^* = 4.52$ meV, which is much larger than $k_BT = 0.17$ meV. Therefore the condition $\hbar\omega_c \gg k_BT$ is satisfied and QO was observed. However for CaAgAs, within the single-band model, $\omega\tau = |\rho_{yx}|/\rho_{xx}$=1.2, which put it at the intermediate-field region and thus QO was not observed at our experiment condition[47]. Based on the Onsager relation, we estimated the Fermi wavevector $k_F = \sqrt{2eF/\hbar}$ to be $0.079\mathring{A}^{-1}$ and the Fermi velocity $v_F = \hbar k_F/m^*$ as 4.0×10^5 m/s. Assuming the oscillations arise from an isotropic Fermi pocket, the carrier density $n = k_F^3/(3\pi^2)$ was estimated as 1.7×10^{25} m^{-3}. This value is 2- 3 times smaller than the ones inferred from Hall and MR data (Fig. 4(c)), suggesting that the associated Fermi surface is not of spherical shape. Our fit also resulted in a $T_D(2\text{K}) = 8.9$ K (Fig. 5(d)) and thus a quantum lifetime $\tau_q(2\text{K}) = 1.4 \times 10^{-13}$ s. Since τ_q arises from all scattering channels which broaden the Landau levels, while the transport lifetime $\tau_{tr} = m^*\mu/e$ mainly arises from backscattering, to investigate if there is a strong suppression of backscattering as is the case for Cd_3As_2[34], we compared τ_q and τ_{tr}. Our estimation of τ_{tr} is quite rough due to the existence of two types of charge carriers and multiple Fermi pockets. Using the m^* and the average of μ_e and μ_h, the estimated τ_{tr} is around 6.5 $\times 10^{-13}$ s and the ratio of τ_{tr}/τ_q is around 4.6. This ratio is significantly smaller than 10^4 in Cd_3As_2[34].

To map out the electronic structure of CaCdGe experimentally, we studied the angle-dependent SdH oscillations. Figures 6 (a) and (b) present the angular dependence of F_a^{SdH}, with the measurement geometries shown in the insets. F_a^{SdH} shows a 6-fold rotational symmetry with the ratio between the maxima and minima being 1.028 (Fig. 6 (b)). This is consistent with its hexagonal crystal structure and indicates small in-plane anisotropy of the associated Fermi pocket.

Figures 6(c) and (d) present the calculated band structures of CaCdGe using the LDA/GGA and MBJ potentials respectively. Regardless of the choice of potential, an extra trivial band (red), besides the nontrivial band carrying the nodal-line feature as proposed in CaAgAs (black), also crosses the FL in CaCdGe . Therefore, both calculations support the electron-hole compensation effect suggested in Fig. 4(c) and (d). However, although Fig. 6(c) and (d) are quite similar in general, they differ in the details, which results in significant differences in the size and topology of the Fermi pockets. We were unable to relate F_a^{SdH} with any Fermi pockets arising from the LDA/GGA band structure shown in Fig. 6(c) since all pockets are very large. On the other hand, the size of F_a^{SdH} matches well with the ovoid-like β Fermi pocket in Fig. 6(e), which originates from the trivial red band when the MBJ potential is used. The comparison between the F_a^{SdH} (yellow lines) and the oscillation frequency associated with the β pocket, F_β^{SdH} (black lines) is shown in Fig. 6(a) and (b). We notice that al-

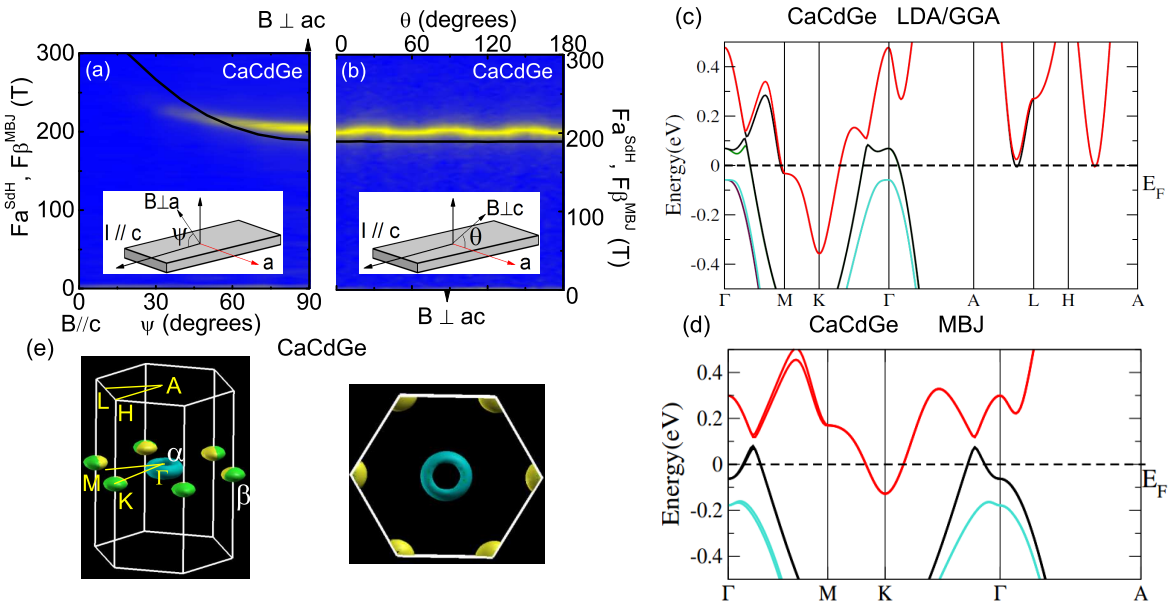

FIG. 6. (a, b) Angular dependence of the experimental F_a^{SdH} (yellow lines; see text) and the calculated F_β^{SdH} (black lines; see text) with the measurement geometries in the insets. (c, d) The electronic band structure of CaCdGe with SOC: (c) Using the LDA/GGA potential. (d) Using the MBJ potential. (e) The Fermi pockets associated with (d).

though the magnitudes of both frequencies match quite well, F_β^{SdH} shows stronger anisotropy in the *ac* plane but weaker anisotropy in the *ab* plane. Nevertheless, our observation suggests that the MBJ potential gives a better description of the band structure of CaCdGe. This may also be true for CaAgAs. However, the band structure of CaAgAs is much less sensitive to the choice of potentials. The one calculated using the MBJ potential is qualitatively the same as the one obtained using the LDA/GGA potential[48]. Unfortunately, up to 9 T, we did not observe frequencies associated with the donut-like α Fermi pocket which originates from the band featuring the nodal-line. Higher magnetic field may be needed to fully unravel the Fermiology of CaCdGe and CaAgAs.

IV. CONCLUSION

In conclusion, we have grown and characterized the single crystalline Dirac nodal-line semimetal candidates CaAgAs and CaCdGe. Magnetoresistance, Hall measurements and first-principles calculations indicate that CaAgAs is a single band material with one donut-like hole Fermi pocket, consistent with the proposal of being the first "hydrogen atom" nodal-line semimetal. First-principles calculations with the MBJ potential show that CaCdGe has one donut-like hole Fermi pocket originating from the band with the nodal-line feature and one trivial ovoid-like electron Fermi pocket. As a result, their magnetotransport properties behave quite differently. At 2 K and 9 T, linear transverse magnetoresistance (MR) up to 18% is observed in CaAgAs while extremely large non-saturating quadratic MR up to 3200% appears in CaCdGe, suggesting that the electron-hole compensation effect is responsible for the extremely large MR observed in CaCdGe. Angle-dependent SdH oscillations in CaCdGe resolve a Fermi pocket with oscillation frequency of 204 T and effective mass of 0.23 m_e, which agrees well with the ovoid-like electron Fermi pocket revealed by the first-principles calculations with the MBJ potential.

V. ACKNOWLEDGMENTS

Work at UCLA was supported by the U.S. Department of Energy (DOE), Office of Science, Office of Basic Energy Sciences under Award Number DE-SC0011978. Work at Rutgers was supported by the NSF DMREF program under the award NSF DMREF project DMR-1435918. T. R. C. is supported by the Ministry of Science and Technology and National Cheng Kung University, Taiwan. T. R. C. also thanks National Center for Theoretical Sciences (NCTS), Taiwan for technical support. We thank Chang Liu for useful discussions.

* These authors contribute equally.

† Corresponding author: nini@physics.ucla.edu

[1] D. Hsieh, D. Qian, L. Wray, Y. Xia, Y. S. Hor, R. J. Cava and M. Z. Hasan, Nature **452**, 970 (2008)

[2] Y. Xia, D. Qian, D. Hsieh, L. Wray, A. Pal, H. Lin, A. Bansil, D. Grauer, Y. S. Hor, R. J. Cava and M. Z. Hasan, Nat. Phys. **5**, 398 (2009)

[3] S. Y. Xu, C. Liu, N. Alidoust, M. Neupane, D. Qian, I. Belopolski, J.D. Denlinger, Y.J. Wang, H. Lin, L.A. Wray et al., Nat. Commun. **3**, 1192 (2012)

[4] H. Lin, R. S. Markiewicz, L. A. Wray, L. Fu, M. Z. Hasan and A. Bansil, Phys. Rev. Lett. **105** , 036404 (2010)

[5] Z. K. Liu, B. Zhou, Y. Zhang, Z. J. Wang, H. M. Weng, D. Prabhakaran, S.-K. Mo, Z. X. Shen, Z. Fang, X. Dai et al., Science, **343**, 864 (2014)

[6] J. Xiong, S. K. Kushwaha, T. Liang, J. W. Krizan, M. Hirschberger, W. Wang, R. J. Cava, N. P. Ong, Science **350**, 413-416 (2015)

[7] S. Borisenko,Q. Gibson, D. Evtushinsky, V. Zabolotnyy, B. Buchner, and R. J. Cava, Phys. Rev. Lett. **113**, 027603 (2014)

[8] M. Neupane, S.-Y. Xu, R. Sankar, N. Alidoust, G. Bian, C. Liu, I. Belopolski, T.-R. Chang, H.-T. Jeng, H. Lin et al., Nat. Commun. **5**, 3786 (2014)

[9] S. Y. Xu, I. Belopolski, N. Alidoust, M. Neupane, G. Bian, C. Zhang, R. Sankar, G. Chang, Z. Yuan, C.-C. Lee et al., Science, **349**, 613-617 (2015)

[10] B. Q. Lv, H.M. Weng, B.B. Fu, X.P. Wang, H. Miao, J. Ma, P. Richard, X.C. Huang, L.X. Zhao, G.F. Chen et al., Phys. Rev. X **5**, 031013 (2015)

[11] Y. Wang, R. M. Nandkishore, Phys. Rev. B **95**, 060506(R) (2017)

[12] S. Sur, R. Nandkishore, New J. Phys. **18**, 115006 (2016)

[13] R. Nandkishore, Phys. Rev. B **93**, 020506(R) (2016)

[14] H. Weng, Y. Liang, Q. Xu, R. Yu, Z. Fang, X. Dai and Y. Kawazoe, Phys. Rev. B **92**, 045108 (2015)

[15] Y. H. Chan, C. K. Chiu, M. Y. Chou and A.P. Schnyder, Phys. Rev. B. **93** 205132 (2016)

[16] M. Zeng, C. Fang, G. Chang, Y.-A. Chen, T. Hsieh, A. Bansil, H. Lin, L. Fu, arXiv:1504.03492v1, Unpublished, (2015)

[17] Y. Kim, B. J. Wieder, C. L. Kane, A. M. Rappe, Phys. Rev. Lett. **115**, 036806 (2015)

[18] Q.-F. Liang, J. Zhou, R.Yu, Z. Wang and H. Weng , Phys. Rev. B **93**, 085427 (2016)

[19] G. Bian, T.-R. Chang, R. Sankar, S.-Y. Xu, H. Zheng, T. Neupert, C.-K. Chiu, S.-M. Huang, G. Chang, I. Belopolski et al., Nat. Commun. **7**, 10556 (2016)

[20] M. M. Hosen, K. Dimitri, I. Belopolski, P. Maldonado, R. Sankar, N. Dhakal, G. Dhakal, T. Cole, P. M. Oppeneer, D. Kaczorowski et al., Phys. Rev. B **95**, 161101(R) (2017)

[21] Y. Chen, Y.-M. Lu and H.-Y. Kee, Nat. Commun. **6**, 6593 (2015)

[22] D. Gosalbez-Martinez, I. Souza and D. Vanderbilt, Phys. Rev. B **92**, 085138 (2015)

[23] L. M. Schoop, M. N. Ali, C. Straer, A. Topp, A. Varykhalov, D. Marchenko, V. Duppel, S. S. P. Parkin, B. V. Lotsch and C. R. Ast, Nat. Commun. **7**, 11696 (2016)

[24] Jin Hu, Z. Tang, J. Liu, X. Liu, Y. Zhu, D. Graf, K. Myhro, S. Tran, C. N. Lau, J. Wei and Z. Mao, Phys. Rev. Lett. **117**, 016602 (2016)

[25] Mewis, A., Revue de Chimie Minerale, **24**, 28-32,(1987)

[26] A. Yamakage, Y. Yamakawa, Y. Tanaka, Y. Okamoto, J. Phys. Soc. Jpn. **85**, 013708 (2016)

[27] Y. Okamoto, T. Inohara, A. Yamakage, Y. Yamakawa and K. Takenaka, J. Phys. Soc. Jpn. **85**, 123701 (2016)

[28] Iandelli, A., Revue de Chimie Minerale,**24**,28-32,(1987)

[29] Blaha, P., Schwarz, K., Madsen, G., Kvasnicka, D. and Luitz, J. WIEN2k, An augmented Plane Wave + Local Orbitals Program for Calculating Crystal Properties. (Techn. Universitat Wien, Austria, 2001).

[30] J. P. Perdew, K. Burke, and M. Ernzerhof, Phys. Rev. Lett. **77**, 3865 (1996).

[31] F. Tran and P. Blaha, Phys. Rev. Lett. **102**, 226401 (2009)

[32] C. L. Zhang, S.-Y. Xu, I. Belopolski, Z. Yuan, Z. Lin, B. Tong, G. Bian, N. Alidoust, C.-C. Lee, S.-M. Huang, T.-R. Chang et al., Nat. Commun. **7**, 10735 (2016)

[33] X. Huang, L. Zhao, Y. Long, P. Wang, D. Chen, Z. Yang, H. Liang, M. Xue, H. Weng, Z. Fang, X. Dai, and G. Chen , Phys. Rev. X **5**, 031023 (2015)

[34] T. Liang, Q. Gibson, M. N. Ali, M. Liu, R. J. Cava and N. P. Ong, Nat. Mater. **14**, 280-284 (2015)

[35] M. N. Ali, J. Xiong, S. Flynn, J. Tao, Q. D. Gibson, L. M. Schoop, T. Liang, N. Haldolaarachchige, M. Hirschberger, N. P. Ong and R. J. Cava, Nature **514**, 205-208 (2014)

[36] B. Shen, X. Y. Deng, G. Kotliar, and N. Ni, Phys. Rev. B **93**, 195119 (2016)

[37] C. Shekhar, A. K. Nayak,Y. Sun, M. Schmidt, M. Nicklas, I. Leermakers, U. Zeitler, Y. Skourski, J. Wosnitza, Z. Liu, Y. Chen, et al., Nat.Phys. **11**, 645-649 (2015)

[38] Y. Zhao, H. Liu, C. Zhang, H.Wang, J. Wang, Z. Lin, Y. Xing, H. Lu, J. Liu, Y. Wang et al., Phys. Rev. X **5**, 031037 (2015)

[39] Y. Zhao, H. Liu, J. Yan, W. An, J. Liu, X. Zhang, H. Wang, Y. Liu, H. Jiang, Q. Li et al., Phys. Rev. B **92**, 041104(R) (2015)

[40] J. Xiong, S. Kushwaha, J. Krizan, T. Liang, R. J. Cava, N. P. Ong, Europhys. Lett. **114**, 27002 (2016)

[41] A. Narayanan, M.D. Watson, S.F. Blake, N. Bruyant, L. Drigo, Y.L. Chen, D. Prabhakaran, B. Yan, C. Felser, T. Kong et al., Phys. Rev. Lett. **114**, 117201 (2015)

[42] Y. Xing, H. Wang, C.-K.i Li, X. Zhang, J. Liu, Y. Zhang, J. Luo, Z. Wang, Y. Wang, L. Ling et al., npj Quant. Mater. **1**, 16005 (2016)

[43] R. Xu, A. Husmann, T.F. Rosenbaum, M.-L. Saboungi, J. E. Enderby and P. B. Littlewood, Nature **390**, 57-60 (1997)

[44] T. Khouri, U. Zeitler, C. Reichl, W. Wegscheider, N. E. Hussey, S. Wiedmann and J. C. Maan, Phys. Rev. Lett. **117**, 256601 (2016)

[45] J. Hu and T. F. Rosenbaum, Nat. Mat. **7**, 697-700 (2008)

[46] A. B. Pippard, Magnetoresistance in Metals (Cambridge, Cambridge, 1989).

[47] C. M. Hurd, The Hall Effect in Metals and Alloys (Plenum Press, New York, 1972).

[48] See Supplemental Material at URL for the MBJ band calculation of CaAgAs.